Organic & Biomolecular Chemistry

PAPER

View Article Online
View Journal | View Issue

Cite this: *Org. Biomol. Chem.*, 2014, **12**, 9621

Synthesis and evaluation of new ^{18}F-labelled acetamidobenzoxazolone-based radioligands for imaging of the translocator protein (18 kDa, TSPO) in the brain†

Anjani K. Tiwari,[a,b] Masayuki Fujinaga,[a] Joji Yui,[a] Tomoteru Yamasaki,[a] Lin Xie,[a] Katsushi Kumata,[a] Anil K. Mishra,[b] Yoko Shimoda,[a] Akiko Hatori,[a] Bin Ji,[a] Masanao Ogawa,[a,c] Kazunori Kawamura,[a] Feng Wang[d] and Ming-Rong Zhang*[a]

Received 12th September 2014,
Accepted 1st October 2014

DOI: 10.1039/c4ob01933d

www.rsc.org/obc

The visualization of the activated microglia/TSPO is one of the main aspects of neuroimaging. Here we describe two new ^{18}F-labelled molecules, 2-[5-(4-[^{18}F]fluoroethoxyphenyl)- ([^{18}F]**2**) and 2-[5-(4-[^{18}F]fluoropropyloxyphenyl)- ([^{18}F]**3**) -2-oxo-1,3-benzoxazol-3(2*H*)-yl]-*N*-methyl-*N*-phenylacetamide as novel PET ligands for imaging the translocator protein (18 kDa, TSPO) in the brain. The three-D pharmacophore evaluation and docking studies suggested their high affinity for the TSPO and *in vitro* binding assays of the TSPO showed binding affinities 6.6 ± 0.7 nM and 16.7 ± 2.5 nM for **2** and **3**, respectively. The radiochemical yields for [^{18}F]**2** and [^{18}F]**3** were found to be 22 ± 4% (n = 8) and 5 ± 2% (n = 5), respectively at EOB. The radiochemical purity for both was found ≥98% and the specific activity was in the range of 98–364 GBq μmol^{-1} at EOS. *In vitro* autoradiography with an ischemic rat brain showed significantly increased binding on the ipsilateral side compared to the contralateral side. The specificity of [^{18}F]**2** and [^{18}F]**3** for binding TSPO was confirmed using the TSPO ligands PK11195 and MBMP. The biodistribution patterns of both PET ligands were evaluated in normal mice by 1 h dynamic PET imaging. In the brain, regional radioactivity reached the maximum very rapidly within 0–4 min for both ligands, similar to (*R*)[^{11}C]PK11195. The metabolite study of [^{18}F]**2** also favoured a more favourable profile for quantification in comparison to (*R*)[^{11}C]PK11195. In summary, these data indicated that [^{18}F]**2** and [^{18}F]**3** have good potential to work as PET ligands, therefore there are merits to use these radioligands for the *in vivo* evaluation in animal models to see their efficacy in the living brain.

Introduction

One of the most focused study for positron emission tomography (PET) imaging is the activation of microglial cells, which is accompanied by the expression of the translocator protein (18 kDa, TSPO) during acute or chronic neuroinflammation.[1,2] The levels of TSPO increase markedly during neuroinflammation and neurodegeneration. Moreover, it has been demonstrated that TSPO functions may be important in modulating neuronal damage and hence, may support accelerated microglial activation for immune responses in such conditions.

The first clinical prototype of a PET ligand specific for TSPO was [^{11}C]PK11195 (Fig. 1);[3] however, its limitations include high lipophilicity, low *in vivo* specific binding and an unfavourable metabolic profile for receptor quantification.[4] These limitations motivated investigators to develop new TSPO PET ligands. Up to date various new radioligands with superior imaging characteristics have been developed, and promising candidates were used in clinical human studies, such as [^{11}C]DAA1106,[5] [^{18}F]FEDAA1106,[6] [^{11}C]PBR28,[7] [^{11}C]AC-5216[8] and [^{18}F]DPA714[9] (Fig. 1). Most of these radioligands bind TSPO with a high affinity in small animals; however, their specific binding is reduced in the human brain.[10,11] Moreover, PBR28 exhibited a mixed affinity with TSPO in "binder" and "non-binder" human subjects.[12–14]

To develop a more appropriate PET ligand, recently we developed a novel ^{11}C-labelled acetamidobenzoxazolone skeleton, 2-[5-(4-[^{11}C]methoxyphenyl)-2-oxo-1,3-benzoxazol-3(2*H*)-yl]-

[a]*Molecular Imaging Centre, National Institute of Radiological Sciences, Inage-ku, Chiba 263-8555, Japan. E-mail: zhang@nirs.go.jp; Fax: +81 43 206 3261; Tel: +81 43 382 3709*
[b]*Division of Cyclotron and Radiopharmaceutical Sciences, Institute of Nuclear Medicine and Allied Sciences, Brig. S. K. Mazumdar Road, Delhi-110054, India*
[c]*SHI Accelerator Service Co. Ltd, Shinagawa-ku, Tokyo 141-8686, Japan*
[d]*Department of Nuclear Medicine, Nanjing Hospital, Affiliated to Nanjing Medical University, Nanjing, China*
†Electronic supplementary information (ESI) available. See DOI: 10.1039/c4ob01933d

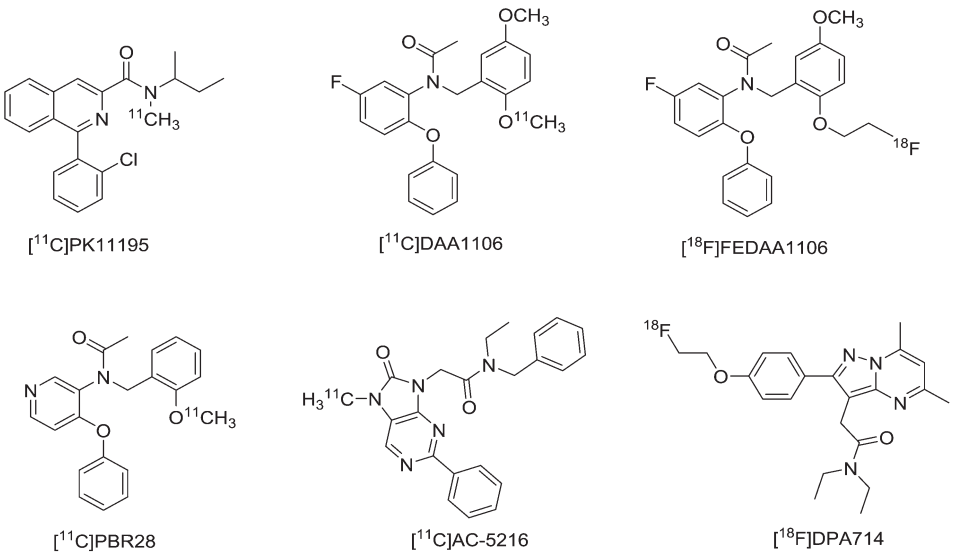

Fig. 1 Representative structures of the TSPO ligands used in clinical PET studies.

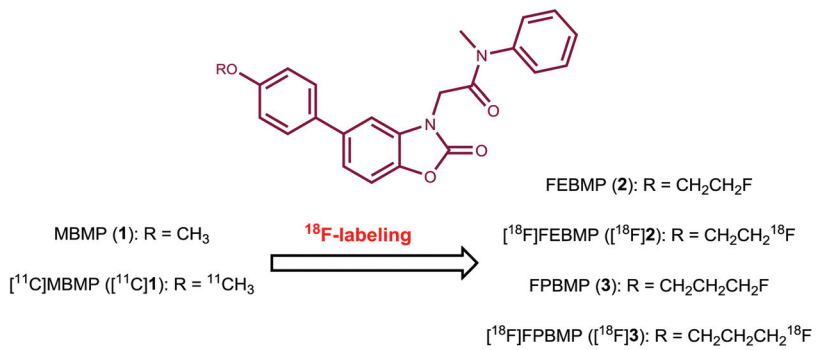

Fig. 2 Development of ^{18}F-ligands for the TSPO.

N-methyl-*N*-phenylacetamide ([^{11}C]MBMP, [^{11}C]**1**; Fig. 2) that binds TSPO *in vitro* with a high affinity and specificity in an ischemic rat brain.[15] However, approximately 20% of the input of [^{11}C]**1** was detected as a metabolite in mice brains 60 min after injection, which hindered its further evaluation and application without further optimization, such as using a different radioisotope and modifying the linker positions.

To address this issue, we synthesized the ^{18}F-labelled analogues of [^{11}C]**1** as putative TSPO ligands for PET as follows: 2-[5-(4-[^{18}F]fluoroethoxyphenyl)- ([^{18}F]FEBMP, [^{18}F]**2**) and 2-[5-(4-[^{18}F]-fluoropropyloxyphenyl)- ([^{18}F]FPBMP, [^{18}F]**3**) -2-oxo-1,3-benzoxazol-3(2*H*)-yl]-*N*-methyl-*N*-phenylacetamide (Fig. 2). Because of the molecular similarity and bioisosteric property of *O*-CH_2CH_2F and *O*-$CH_2CH_2CH_2F$ with *O*-CH_3 groups, compounds **2** and **3** may display similar affinities for TSPO with **1**. Compounds **1–3** are lipophilic and therefore may pass readily through the blood-brain barrier (BBB). Moreover, the [^{18}F]fluoroalkoxy substitution may improve the pharmacokinetics and metabolism,[16] and the longer half-life (110 min *vs.* 20 min) of ^{18}F allows time for complex chemical syntheses and emits lower positron energy (650 KeV *vs.* 960 KeV), which is appropriate for convenient long-term storage as well as for transportation to distant research and clinical facilities. Here, we report the radiosynthesis of two new radioligands [^{18}F]**2** and [^{18}F]**3** and the evaluation of their potential in PET imaging of the TSPO in the brain.

Results and discussion

Chemistry

Two novel fluoroalkoxy analogues, **2** and **3**, were synthesized by heating precursor **4** [15] with the respective tosylates **5** and **6**, which were synthesized by reacting alcohols **7** and **8** with 4-methylbenzenesulfonyl chloride in the presence of K_2CO_3 at 70 °C for 4–6 h (Scheme 1). Their respective yields ranged from 59% to 65%. The chemical purities of these compounds were determined using HPLC (ESI Fig. 1†). (*R*)[^{11}C]PK11195 was synthesized as per previous literature.[3] The radiochemical purity of (*R*)[^{11}C]PK11195 was 99% and the specific activity was calculated as 74 ± 8 GBq μmol^{-1} (n = 3) at EOS.

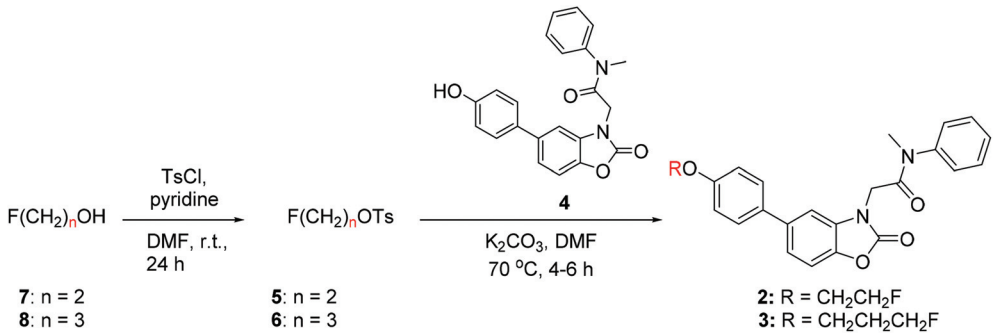

Scheme 1 Chemical synthesis of **2** and **3**.

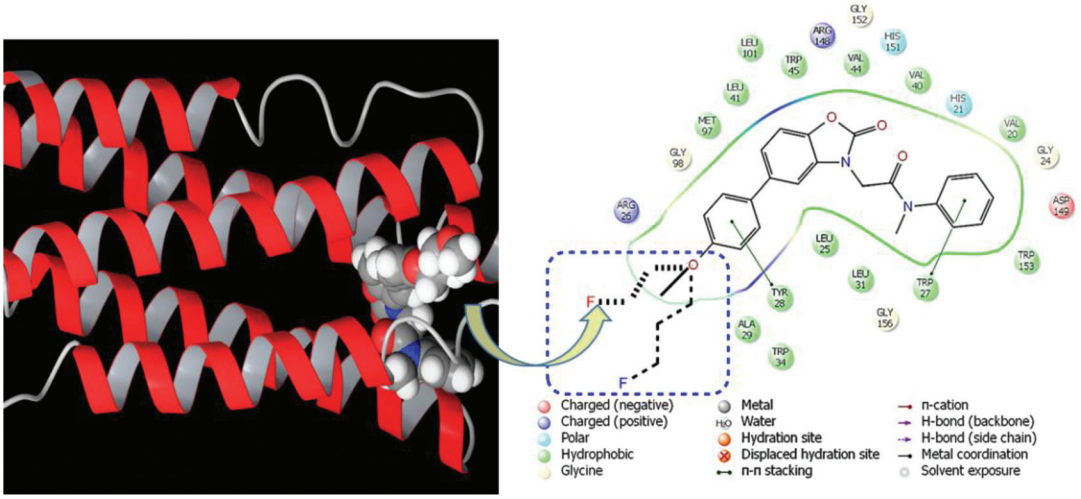

Fig. 3 2D/3D TSPO–ligand interactions.

Computational docking of receptor-ligand binding analysis

The ligand–protein interaction through the docking analysis of molecules **1–3** confirmed short-range interactions with TSPO, including π–π interactions among the aromatic residues such as Tyr28, Trp27, Phe19 and Trp99. These molecules were buried in the hydrophobic pocket in the transmembrane region (Fig. 3). Compounds **1–3** exhibit similar pharmacophore features and interactions with the binding pocket of the TSPO. This was confirmed by the Gscore of docking (ESI Table 1†) and the same interactions with the amino acid residues in the diagrams of the 2D and 3D ligand–protein interactions. These promising data prompted us to analyse these ligands for *in vitro* receptor binding.

In vitro binding assay

We used rat brain homogenates to determine the inhibition constants (K_i) of compounds **1–3** for the TSPO by measuring the competition for binding with (*R*)[^{11}C]PK11195, which is a selective radioligand for TSPO in the concentration range of 0.1 nM to 10 μM (Fig. 4). These data showed that the percentage of specific binding was around 80% for compounds **1–3**. Further K_i was calculated as shown in Table 1, and **2** and **3** bind TSPO with a high (nanomolar) affinity, thus confirming the results of the computer modelling study. In particular, **2** bound TSPO with a similar affinity to that of **1** and PK11195, suggesting that substituting *O*-CH_3 with *O*-CH_2CH_2F in the

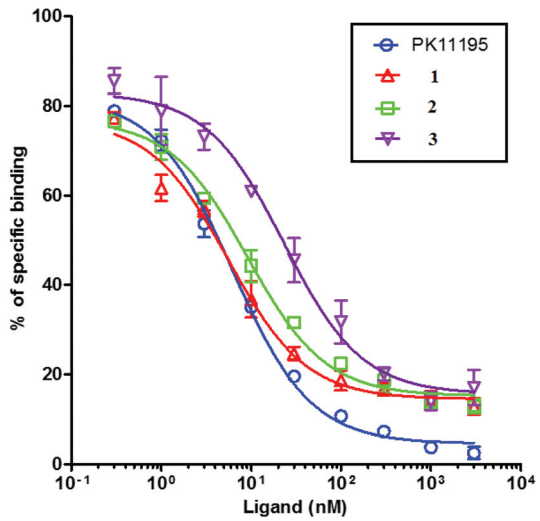

Fig. 4 Competitive binding curves for the novel TSPO ligands.

Table 1 *In vitro* binding affinity for the TSPO and the lipophilicity of compounds **1–3**

Compound	Binding affinity (K_i) TSPO[a]	Lipophilicity: Experimentally measured log D[b]	Lipophilicity: Calculated c log D[c]
2	6.6 ± 0.7	3.4	3.5
3	16.7 ± 2.5	3.5	3.7
1	3.9 ± 0.6	3.4	3.3
PK11195	4.4 ± 0.4	3.7	5.1

[a] Binding affinities represent the mean ± standard error of the mean (SE) of triplicate samples of brain homogenates. [b] log D values were measured in octanol/phosphate buffer (pH = 7.4) using the shake flask method (n = 3; maximum range, ± 5%). [c] c log D values were calculated using the Pallas 3.4 software.

benzene ring did not significantly alter its affinity for the TSPO. The substitution of *O*-CH_3 with *O*-$CH_2CH_2CH_2F$ decreased its affinity. However, this level of binding affinity for **3** was considered appropriate for imaging brain receptors according to the results of our previous study.[17]

The computed lipophilicities at pH = 7.4 (c log D) of [^{18}F]**2** and [^{18}F]**3** were 3.4 and 3.5, respectively, and the corresponding experimental values of 3.5 and 3.7 (log D) were determined using the shake flask method (Table 1).[18] The lipophilicity values of both ligands were similar to that of [^{11}C]**1** and lower than that of (*R*)[^{11}C]PK11195, indicating that they may permeate the BBB as predicted for [^{11}C]**1**.

Radiochemistry

Two [^{18}F]fluoroalkoxy ligands [^{18}F]**2** and [^{18}F]**3** were synthesized by reacting **4** with 1-bromo-2-[^{18}F]fluoroethane ([^{18}F]**9**) or 1-bromo-3-[^{18}F]fluoropropane ([^{18}F]**10**), respectively (Scheme 2). These labelling agents were prepared by [^{18}F]fluorination of 2-bromoethyltrifluoromethanesulfonate (**11**) or 3-bromopropyltrifluoromethanesulfonate (**12**) with [^{18}F]F^- using a synthetic unit developed in our laboratory.[19] A solution of **11** or **12** in 1,2-dichlorobenzene was added to dry [^{18}F]F^-, and the reaction mixture was immediately heated to produce [^{18}F]**9** or [^{18}F]**10**, which was distilled, dried and trapped in a solution of **4** and NaOH in DMF. The purification of [^{18}F]**9** (boiling point 71.5 °C) or [^{18}F]**10** (boiling point 101 °C) by distillation achieved a radiochemical purity of >95%.[20] Moreover, this method removed all non-volatile impurities such as metal ions from the cyclotron target, unreacted [^{18}F]F^-, and the phase-transfer catalyst, Kryptofix 222/K_2CO_3. After trapping each reagent, the reaction mixture was heated at 90 °C or 120 °C for 10 min. Following HPLC purification, the radiochemical yields of [^{18}F]**2** and [^{18}F]**3** were 22 ± 4% (n = 8) and 5 ± 2% (n = 5), respectively, and were based on [^{18}F]F^-, which was corrected for physical decay during the reaction times of 64 ± 5 and 61 ± 3 min from the end of bombardment, respectively.

The identities of [^{18}F]**2** and [^{18}F]**3** were confirmed by coinjection with the corresponding unlabelled **2** and **3** using reverse phased-analytical HPLC (ESI Fig. 2†). The radiochemical purities of the final products were >98% and unreacted **4** was not detected in the HPLC chromatograms. Moreover, the final products did not undergo radiolysis at room temperature for 120 min. The analytical results were consistent with our in-house quality specifications of radiopharmaceuticals.

In vitro autoradiography of an ischemic rat brain by using [^{18}F]**2** and [^{18}F]**3**

Because of the low density of the TSPO in a normal brain, a well-characterized ischemic model was used to visualize the *in vitro* binding of [^{18}F]**2** and [^{18}F]**3** to the TSPO. In this model, neuroinflammation accompanied by microglial activation increased the TSPO density in the ischemic area.[21] Fig. 5 shows the *in vitro* autoradiograms of [^{18}F]**2** and [^{18}F]**3** in the ischemic rat brain. In the control section (A), radioactivity was high in the ipsilateral side (right) compared with the contralateral side (left). However, these differences were abolished by incubation with an excess of unlabelled **1** (B) or PK11195 (C).

Quantification of the autoradiograms shows that the ratios of the radioactive signals in the ipsilateral side compared with

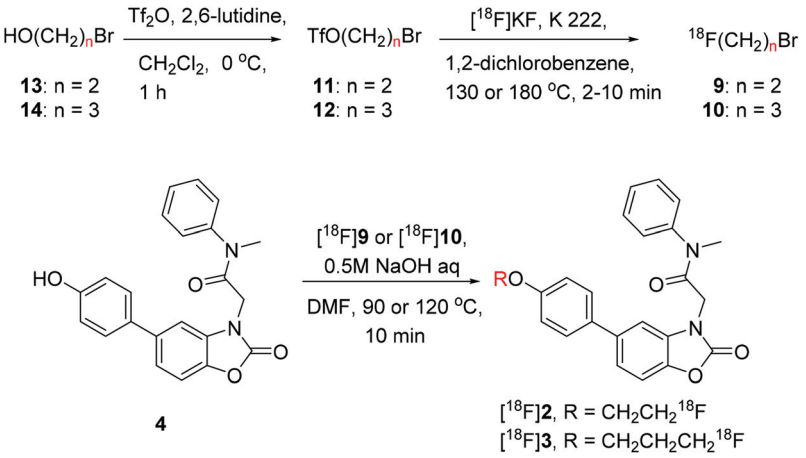

Scheme 2 Radiosynthesis of [^{18}F]**2** and [^{18}F]**3**.

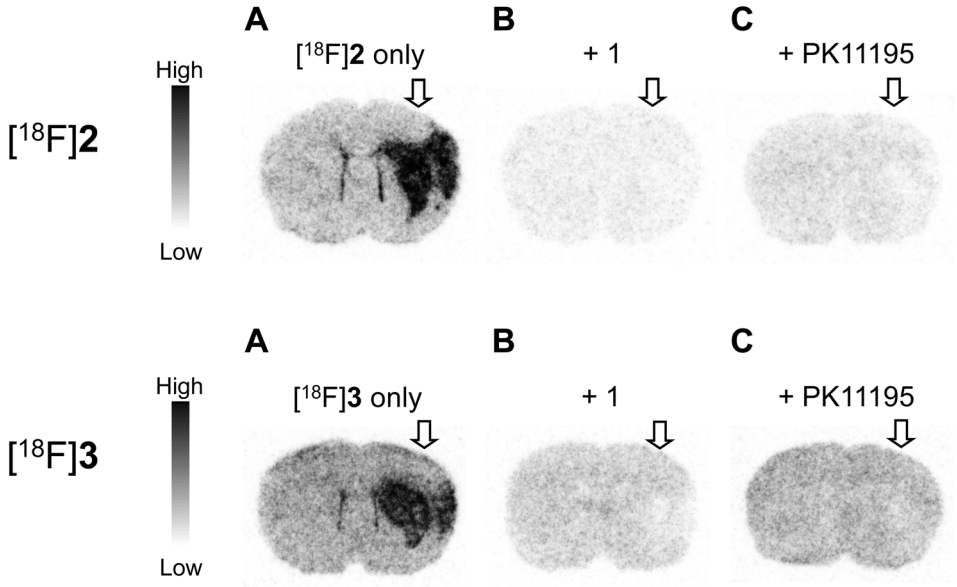

Fig. 5 Representative *in vitro* autoradiograms of [^{18}F]**2** and [^{18}F]**3** in ischemic rat brains (n = 4). Arrows indicate the ischemic areas. (A) [^{18}F]**2** or [^{18}F]**3** only; (B) incubation with unlabelled **1**; (C) incubation with PK11195.

the contralateral side were 3.1 for [^{18}F]**2** and 2.1 for [^{18}F]**3**, and the values for each were approximately 1.0 in the presence of unlabelled **1** or PK11195 (Fig. 6). Compared with the controls ([^{18}F]**2** or [^{18}F]**3** only), competition for the binding of [^{18}F]**2** or [^{18}F]**3** with **1** or PK11195 significantly reduced the ipsilateral binding (−91.2% by **1** and −84.6% by PK11195 competing with [^{18}F]**2**, and −81.2% by **1** and −67.4% by PK11195 competing with [^{18}F]**3**), although it was lower for the contralateral binding (−80.3% by **1** and −67.8% by PK11195 competing with [^{18}F]**2**, and −50.1% by **1** and −23.7% by PK11195 competing for [^{18}F]**3**). These results demonstrate the high *in vitro* specific binding of [^{18}F]**2** and [^{18}F]**3** to the TSPO. Further, [^{18}F]**2** bound TSPO with a higher specificity compared with [^{18}F]**3**.

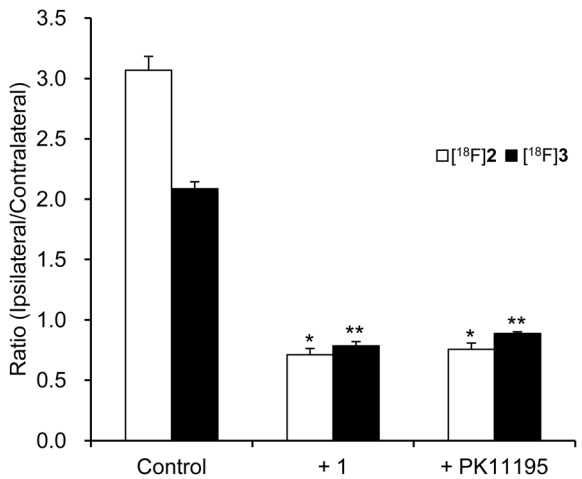

Fig. 6 Quantitation of the autoradiograms of [^{18}F]**2** and [^{18}F]**3**. The concentrations of radioactivity in brain regions are expressed as photostimulated luminescence (PSL) mm^{-2}. *P < 0.05, [^{18}F]**2**: control *vs.* treatment with **1** or PK11195, **P < 0.05, [^{18}F]**3**: control *vs.* treatment with **1** or PK11195.

Analysis of the dynamic PET images

To determine the kinetic parameters related to the distribution and uptake of [^{18}F]**2** and [^{18}F]**3** *in vivo* in comparison to (*R*)[^{11}C]PK11195, dynamic PET imaging was performed. The PET data acquired between 0 and 60 min, 0–4 min, 4–10 min, 10–16 min and 55–60 min were summed, and the images are shown in Fig. 7. The reason for taking more summation at the initial phase, was because both ligands showed a fast uptake in the brain, within a few minutes after injection.

The PET dynamic scans showed the fast accumulation of radioactivity in the brain within 0–4 min and similarly in major TSPO related organs such as the lungs and heart. The biodistribution patterns of [^{18}F]**2** and [^{18}F]**3** were found to be similar to the known PET ligand (*R*)[^{11}C]PK11195. Both PET ligands [^{18}F]**2** and [^{18}F]**3** were able to cross the BBB very rapidly. Further, the uptake in the peripheral organs decreased rapidly till 15 min and after that decreased slowly till 60 min. The uptake value in the kidney reached a maximum and maintained a plateau parallel to the x axis. Comparative time-activity curves (TACs) were also prepared for other organs and for bones (Fig. 8). The TACs data showed that maximum uptake in brain was 2.5%–3.0% ID g^{-1} for [^{18}F]**2** and [^{18}F]**3**, which decreased rapidly till 15 min and reached a level of 1.0% ID g^{-1} at 60 min, similar to (*R*)[^{11}C]PK11195. Bone uptake was also measured for these ligands as they were labelled with ^{18}F. The accumulation of radioactivity in the bone was found to be 1.4% ID g^{-1} for [^{18}F]**3** as compared to 1.2% ID g^{-1} for [^{18}F]**2** at 60 min after the injection (ESI Fig. 3†).

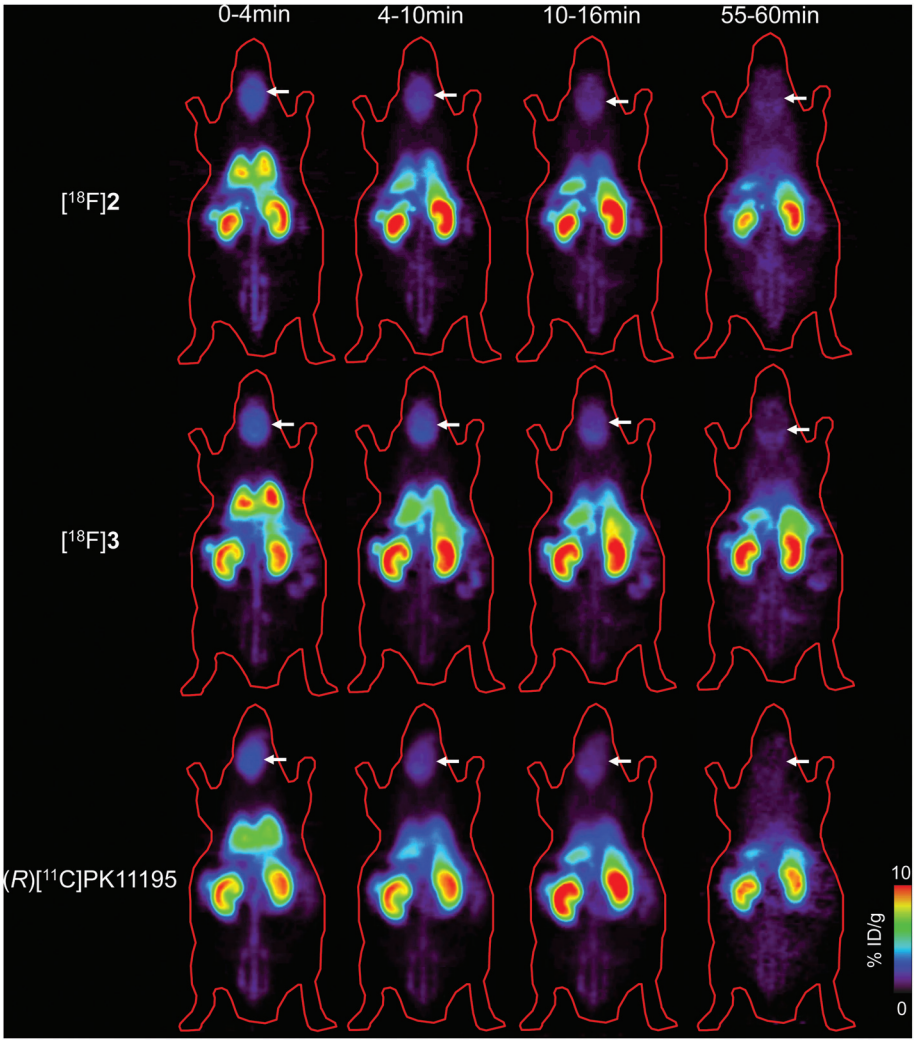

Fig. 7 Dynamic PET images of [^{18}F]**2**, [^{18}F]**3** and (*R*)[^{11}C]PK11195 at different time intervals (0–60 min). Arrows indicate the brains.

Finally, on the basis of the better *in vitro* properties (K_i & autoradiography) and lower bone uptake *in vivo*, [^{18}F]**2** was analysed for metabolic stability.

Determination of radiolabelled metabolites by HPLC

In the brain [^{18}F]**2** showed intactness in the range of 85% to 90% at 15–30 min but in the plasma, the intactness of the original ligand decreased very rapidly. The HPLC charts of [^{18}F]**2** in mice plasma and brains are shown in Fig. 9. Only one polar metabolite during 60 min studies was found in both the plasma and brain. The polarity of this metabolite may not allow it to cross the BBB and even if so, it did not stay in the brain due to its hydrophilicity. This may give a good opportunity to evaluate the specific binding to TSPO in the brain by using the quantification studies of [^{18}F]**2**.

The comparison of the well-known ligand (*R*)[^{11}C]PK11195 with [^{18}F]**2** and [^{18}F]**3** was performed in similar experimental conditions. The *in vitro* autoradiography of (*R*)[^{11}C]PK11195 (ESI Fig. 4†) showed comparable, or even more specific results than [^{18}F]**2** and [^{18}F]**3**. The brain uptake was found similar in the order of [^{18}F]**2** > [^{18}F]**3** > (*R*)[^{11}C]PK11195 (ESI Fig. 5†), which is the main requisite for *in vivo* imaging. On the other hand, a previous study indicated the fast metabolism of [^{11}C]PK11195 in rat plasma along with five radiometabolites.[22] The HPLC analysis showed that the retention time of intact [^{11}C]PK11195 and its radiolabelled non-polar metabolites were very near, which suggested their similar capabilities for crossing the BBB in rats. Compared to (*R*)[^{11}C]PK11195, [^{18}F]**2** was not metabolized into non-polar metabolites in the mice plasma and brain.

Conclusion

The rational design of the new ^{18}F-labelled ligands for the PET imaging of TSPO based on our previous study of a ^{11}C-labelled acetamidobenzoxazolone-based TSPO ligand led to the successful synthesis and high purity preparation of [^{18}F]**2** and

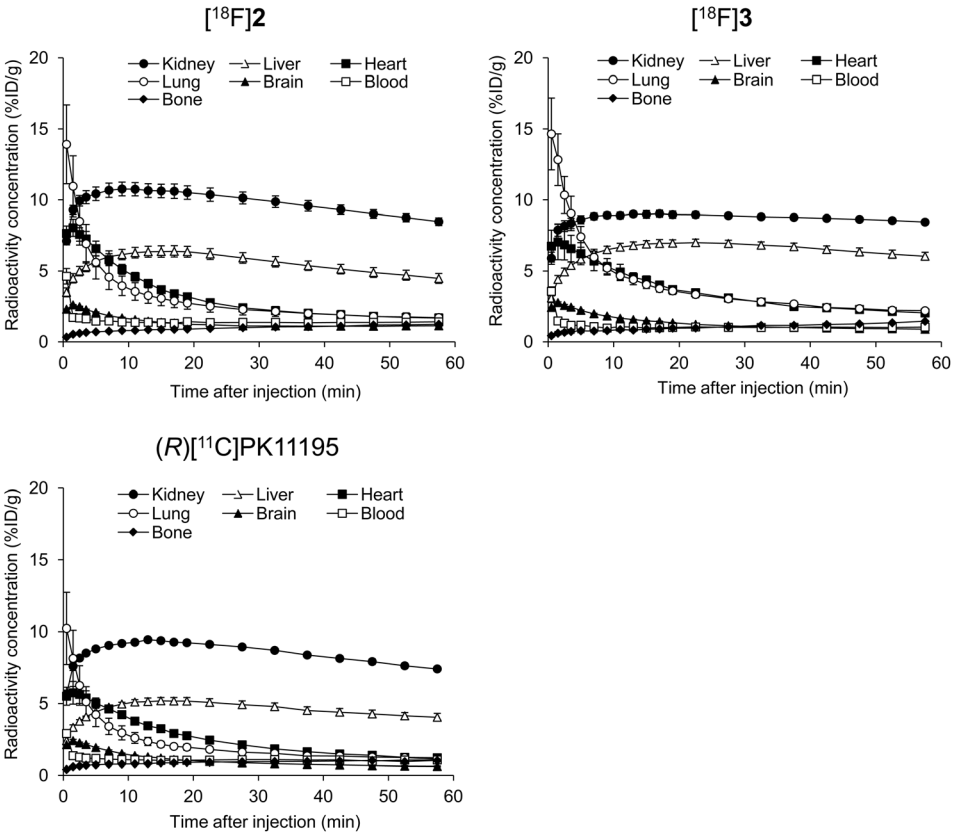

Fig. 8 Time–activity curves of [^{18}F]**2**, [^{18}F]**3** and (*R*)[^{11}C]PK11195 in organs expressed as radioactivity concentration *versus* time.

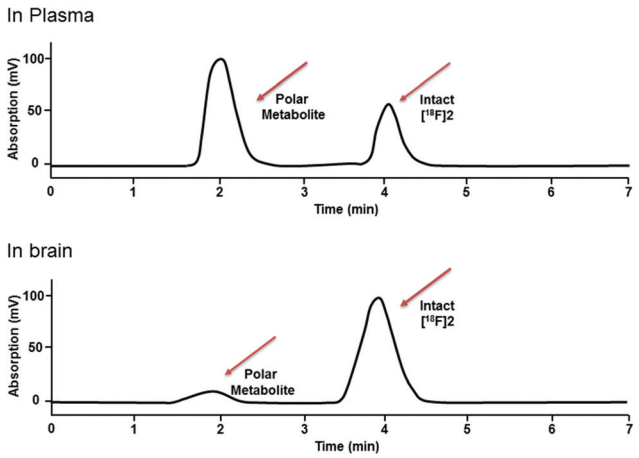

Fig. 9 Representative radio-HPLC chromatograms of mice plasma sample and brain homogenates obtained at 15 min after injection of [^{18}F]**2**.

[^{18}F]**3**. These radioligands were stable and bound TSPO with a high affinity and specificity in an ipsilateral ischemic rat brain *in vitro*. The PET dynamic studies also validated its distribution and selectivity for TSPO in the brain regions. These findings provide a compelling argument for the testing of these novel PET ligands *in vivo* with a particular focus on the brain imaging of putative binders and non-binders.

Experimental section

Chemicals and instrumentation

All chemicals were purchased from commercial sources. Melting points were determined using a Yanaco MP-500P micromelting point apparatus. The ^{1}H-NMR (300 MHz) spectra were recorded using a JEOL-AL-300 NMR spectrometer with tetramethylsilane as an internal standard. The high-resolution fast atom bombardment mass spectra [HRMS(FAB)] were acquired using a JEOL JMS-Sx 102A spectrometer. HPLC separation and analysis were performed using a JASCO HPLC system. Effluent radioactivity was monitored using a NaI (Tl) scintillation detector system, and radioactivity was measured during the synthesis and animal studies using an Aloka Curiemeter. To measure the *in vitro* binding affinity for TSPO, (*R*)[^{11}C]PK11195 was synthesized as described previously.[3]

Chemical synthesis

2-[5-(4-Fluoroethoxyphenyl)-2-oxo-1,3-benzoxazol-3(2*H*)-yl]-*N*-methyl-*N*-phenylacetamide (2). 2-Fluoroethyl 4-methylbenzenesulfonate[18] (**5**, 56 mg, 0.30 mmol) was added to a solution of 2-[5-(4-hydroxyphenyl)-2-oxo-1,3-benzoxazol-3(2*H*)-yl]-*N*-methyl-*N*-phenylacetamide[15] (**4**, 100 mg, 0.27 mmol) and K_2CO_3 (57 mg, 0.41 mmol) in anhydrous DMF (5 mL). The reaction mixture was heated for 4 h at 70 °C, quenched with water and extracted with ethyl acetate. The organic layer was washed with

brine, dried over Na_2SO_4 and evaporated under reduced pressure. The residue was purified using silica gel column chromatography with *n*-hexane–ethyl acetate (1/2, v/v) to give **2** (58 mg, 52.0% yield) as a colourless solid with the properties as follows: mp 170–172 °C; ^{1}H NMR ($CDCl_3$, δ) 3.32 (3H, s), 4.27 (2H, dt, J = 4.2, 27.9 Hz), 4.35 (2H, s), 4.79 (2H, dt, J = 4.0, 47.3 Hz), 6.99–7.02 (3H, m), 7.22 (1H, s), 7.23 (2H, d, J = 8.8 Hz), 7.33–7.36 (2H, m), 7.44–7.54 (5H, m) and HRMS (FAB) $C_{24}H_{22}O_4N_2F$, calculated 421.1564; found, 421.1516.

2-[5-(4-Fluoropropyloxyphenyl)-2-oxo-1,3-benzoxazol-3(2*H*)-yl]-*N*-methyl-*N*-phenylacetamide (3). 2-Fluoropropyl 4-methylbenzenesulfonate[18] (**6**; 70 mg, 0.30 mmol) was added to a solution of **4** (100 mg, 0.27 mmol) and K_2CO_3 (57 mg, 0.41 mmol) in anhydrous DMF (5 mL). The reaction mixture was heated for 6 h at 70 °C, quenched with water and extracted with ethyl acetate. The organic layer was washed with brine, dried over Na_2SO_4 and evaporated under reduced pressure. The residue was purified using silica gel column chromatography with *n*-hexane–ethyl acetate (1/1, v/v) to give **3** (70 mg, 60.2% yield) as a colourless solid with the properties as follows: mp 148–152 °C; ^{1}H-NMR ($CDCl_3$, δ) 2.14–2.27 (2H, m), 3.32 (3H, s), 4.15 (2H, t, J = 6.0 Hz), 4.35 (2H, s), 4.68 (2H, dt, J = 5.7,47.3 Hz), 6.96–6.99 (3H, m), 7.22–7.24 (2H, m), 7.35 (2H, t, J = 6.6 Hz), 7.44–7.54 (5H, m) and HRMS (FAB) calculated for $C_{25}H_{24}O_4N_2F$, 435.1720; found, 435.1703.

Radiosynthesis

2-[5-(4-[^{18}F]Fluoroethoxyphenyl)-2-oxo-1,3-benzoxazol-3(2*H*)-yl]-*N*-methyl-*N*-phenylacetamide ([^{18}F]2). [^{18}O]H_2O (95%) was used for irradiation. [^{18}F]HF was recovered from the cyclotron target, separated from [^{18}O]H_2O, concentrated on a short QMA column and eluted with 400 μL of a solution containing aqueous K_2CO_3 (110 mg/8 mL), Kryptofix®222 (330 mg) in MeCN (8 mL). Aqueous [^{18}F]KF was transferred to a reaction vial and evaporated to remove H_2O and MeCN at 110 °C for 15 min. After **11** (7 μL) in 1,2-dichlorobenzene (150 μL) was added to the vial, the reaction mixture was heated at 130 °C to give [^{18}F]**9**, which was distilled using nitrogen gas (10 mL min^{-1}) for 2 min and trapped in a solution of **4** (1.0 mg) and NaOH (5 μL, 0.5 M) in anhydrous DMF (300 μL) at −15 to −20 °C. After the radioactivity plateaued, the reaction mixture was heated at 90 °C for 10 min. HPLC purification was completed using a mobile phase of MeCN–H_2O–Et_3N (6.0/4.0/0.01, v/v/v) at a flow of 5.0 mL min^{-1}. The radioactive fraction corresponding to the desired product was collected in a sterile flask, evaporated to dryness *in vacuo*, redissolved in 3 mL of sterile normal saline and passed through a 0.22 μm Millipore filter. The t_R of [^{18}F]**2** was 9.7 min for purification and 9.4 min for analysis on HPLC.

2-[5-(4-[^{18}F]Fluoropropyloxyphenyl)-2-oxo-1,3-benzoxazol-3(2*H*)-yl]-*N*-methyl-*N*-phenylacetamide ([^{18}F]3). 12 (10 μL) in 1,2-dichlorobenzene (150 μL) was added to a dried [^{18}F]KF-containing vial. The reaction mixture was heated at 150 °C for 2 min to produce [^{18}F]**10**, which was distilled and trapped in a solution of **4** (1.0 mg) and NaOH (5 μL, 0.5 M) in anhydrous DMF (300 μL) at −15 to −20 °C. After the trapping was complete, the reaction mixture was heated at 120 °C for 10 min. HPLC purification was completed using a mobile phase of MeCN–H_2O–Et_3N (65/35/0.01, v/v/v) at a flow rate of 5.0 mL min^{-1} for [^{18}F]**3**. The t_R of [^{18}F]**3** was 8.8 min for purification and 8.3 min for analysis on HPLC.

Computational analysis

The human TSPO (PBR) sequence was retrieved from the NCBI database. The modelling of the receptor was performed using the Prime Homology Modelling tool (Schrödinger). The docking study was initiated by joining the proteins and ligands. The pharmacophore modelling studies were performed using PHASE, version 3.4, (Schrödinger, LLC, New York, NY 2012).

Measurement and computation of lipophilicity

The log D values were measured by mixing [^{18}F]**2** or [^{18}F]**3** (radiochemical purity, 100%; about 200 000 cpm) with *n*-octanol (3.0 g) and sodium-phosphate buffer (PBS 3.0 g, 0.1 M, pH 7.4) in a test tube, which was vortexed for 3 min at room temperature, followed by centrifugation at 3500 rpm for 5 min. An aliquot of 1 mL PBS and 1 mL *n*-octanol was removed, weighed and counted. Samples from the remaining organic layer were removed and repartitioned until consistent log D values were obtained. The log D value was calculated from the ratio of cpm g^{-1} of *n*-octanol to that of PBS and expressed as log D = log[cpm g^{-1} (*n*-octanol)/cpm g^{-1} (PBS)]. All assays were performed in triplicate.

Animals

Male Sprague-Dawley (SD) rats were purchased from Japan SLC and were maintained in an experimental animal rearing room, which was maintained under optimal conditions with a 12/12 h dark/light cycle and were handled in accordance with the recommendations of the National Institute of Health and institutional guidelines of the National Institute of Radiological Sciences (NIRS). The Animal Ethics Committee of the NIRS approved the experiments conducted at the NIRS.

In vitro assays of TSPO binding

The TSPO binding assay was performed as per the previous literature.[21] Briefly, three rats were sacrificed by cervical dislocation with 5% (v/v) isoflurane anaesthesia. The brains were removed quickly and homogenized in ice-cold Tris-HCl buffer (50 mM, pH 7.4) containing 120 μM NaCl. The homogenate was centrifuged at 40 000*g* for 15 min at 4 °C. Subsequently the supernatant was discarded and then the pellet was resuspended, homogenized, and centrifuged under the same conditions. This procedure was repeated twice. The pellet was resuspended in 50 mM Tris-HCl buffer (pH 7.4) at a concentration of 100 mg of the original wet tissue per mL and used for the binding assays.

The crude mitochondrial preparations (100 μL) were incubated with (*R*)[^{11}C]PK11195 (final concentration 2.5 nM) and various concentrations (0.3 nM–3 μM) of ligands **1–3** and PK11195 in a total volume of 1 mL Tris-HCl buffer at room

temperature for 30 min, and the reaction was terminated by rapid filtration through Whatman GF/C glass fibre filters pretreated with 0.3% polyethylenimine, using an M-24 cell harvester (Brandel). The filters were washed three times with 5 mL of ice-cold Tris-HCl buffer (50 mM), and the filter-bound radioactivity was counted using an auto-gamma scintillation counter. The nonspecific binding was determined using a saturated concentration (10 μM) of PK11195. The K_i for the TSPO of each ligand was determined according to the following equation:

$$K_i = \frac{IC_{50}}{1 + \frac{[L]}{K_d}}$$

where [L] is the concentration of (*R*)[^{11}C]PK11195 (nM). The dissociation constant (K_d) of (*R*)[^{11}C]PK11195 for the TSPO was obtained using the Scatchard plot analysis.

In vitro autoradiography of an ischemic rat brain

Mild focal ischemia in rat brains was produced by intraluminal occlusion of the middle cerebral artery for 30 min using an intraluminal thread model.[23,24] Briefly, a Sprague Dawley rat (8–9 weeks of age, 240–330 g) was anesthetized with 4% (v/v) isoflurane and maintained with 1.8% isoflurane, and the right internal carotid artery was ligated. A 4.0-monofilament nylon suture coated with silicon was inserted (16–18 mm) into the internal carotid artery to the middle cerebral artery branches. The neck incision was closed with a silk suture. After regaining consciousness from the anaesthesia, the rats were anaesthetized again after 30 min, and the filament was carefully removed for reperfusion. Throughout the surgery, the body temperature was monitored and maintained at an optimal level. All rats (n = 4) were employed for experiments 7 days after the surgery.

The coronal sections (10 μm) were prepared from frozen rat brains using a cryostat (HM560, Carl Zeiss, Germany). Brain sections were preincubated for 20 min in 50 mM Tris-HCl buffer (pH 7.4), and the sections were then incubated for 30 min at room temperature in fresh buffer containing [^{18}F]**2** or [^{18}F]**3** (1.5 MBq, 0.08 nM). For the inhibition studies, unlabelled **1** (10 μM) or PK11195 (10 μM) was incubated with [^{18}F]**2** or [^{18}F]**3**. After incubation, the brain sections were washed (3 × 2 min) with cold buffer, dipped in cold distilled water and dried with cold air. The sections were placed in contact with imaging plates (BAS-MS2025, Fujifilm), and the autoradiograms were analysed using a bio-imaging system (BAS5000, Fujifilm). The concentrations of radioactivity determined in the brain sections were expressed as photo-stimulated luminescence (PSL) mm^{-2}.

PET study and image analysis

A small-animal PET scanner from Siemens Medical Solutions, was used for imaging. Normal mice were anesthetized during the scan and the animals' body temperature was maintained with a 40 °C water circulation system (T/Pump TP401, Gaymar Industries). The emission scans were acquired at different time intervals after the injection of [^{18}F]**2** (5.18 ± 0.29 MBq/0.02–0.04 nmol), [^{18}F]**3** (4.85 ± 0.17 MBq/0.018–0.034 nmol) and (*R*)[^{11}C]PK11195 (37.0 MBq ± 2.0 MBq/0.02–0.04 nmol) through the tail vein. All image frames were summed and the regions of interest (ROI) were drawn over the brain, heart, liver, spleen, kidneys, stomach and bone of each mouse within four time intervals of 0–4 min, 4–10 min, 10–16 min and 55–60 min. The time activity curves (TACs) for the brain, heart, blood, kidney, lung, liver and bone were generated from the dynamic PET data in order to parameterize the radioactivity uptake, clearance and distribution in healthy mice. The radioactivity (% ID g^{-1}) was estimated as the ratio of the regional activity concentration normalized by the injected dose and the weight of the animal to give the PET-generated biodistribution pattern over various critical organs.

The data modelling for the PET scans was performed into three-dimensional (3D) sinograms, which were changed into two-dimensional (2D) sinograms by Fourier rebinning. Dynamic image reconstruction was done by filtered back-projection using the Hanning's filter with a Nyquist cut-off frequency of 0.5 cycle per pixel. The PET images were analyzed using ASIPro VM™ (Analysis Tools and System Setup/Diagnostics Tool; Siemens Medical Solutions) with reference to the MR imaging template.

Radiolabelled metabolite analysis

The ddY mice were intravenously injected with [^{18}F]**2** (7.4 MBq per mouse) through the tail vein. The animals were sacrificed by cervical dislocation at 5, 15, 30 or 60 min (n = 3 for each point). Blood (0.7–1.0 mL) and entire brain samples were obtained and treated as reported previously.[15] The supernatant of the plasma and brain homogenate was analyzed according to the following conditions: Capcell Pack UG80 C_{18} column, 4.6 mm i.d. × 250 mm; MeCN–H_2O–Et_3N, 7/3/0.01 (v/v/v); flow rate, 1.0 mL min^{-1}. The percentages of the unchanged [^{18}F]**2** were calculated, and at the same time, the radioactivity fractions in the HPLC waste solution were measured using a 1480 Wizard 3" auto-gamma counter.

Acknowledgements

The authors thank the staff of the National Institute of Radiological Sciences for their support for radiosynthesis and animal experiments. In addition the first author would like to thank the Japan Society for the Promotion of Science for support.

References

1 V. Papadopoulos, M. Baraldi, T. R. Guilarte, T. B. Knudsen, J. J. Lacapère, P. Lindemann, M. D. Norenberg, D. Nutt, A. Weizman, M. R. Zhang and M. Gavish, *Trends Pharmacol. Sci.*, 2006, **27**, 402–409.

2 P. Casellas, S. Galiegue and A. S. Basile, *Neurochem. Int.*, 2002, **40**, 475–486.
3 R. Camsonne, C. Crouzel, D. Comar, M. Maziere, C. Prenant, J. Sastre, M. A. Moulin and A. Syrota, *J. Labelled Compd. Radiopharm.*, 1984, **21**, 985–991.
4 F. Chauveau, H. Boutin, N. Van Camp, F. Dollé and B. Tavitian, *Eur. J. Nucl. Med. Mol. Imaging*, 2008, **35**, 2304–2319.
5 M. R. Zhang, T. Kida, J. Noguchi, K. Furutsuka, J. Maeda, T. Suhara and K. Suzuki, *Nucl. Med. Biol.*, 2003, **30**, 513–519.
6 M. R. Zhang, J. Maeda, M. Ogawa, J. Noguchi, T. Ito, Y. Yoshida, T. Okauchi, S. Obayashi, T. Suhara and K. Suzuki, *J. Med. Chem.*, 2004, **47**, 2228–2235.
7 E. Briard, S. S. Zoghbi, M. Imaizumi, J. P. Gourley, H. U. Shetty, J. Hong, V. Cropley, M. Fujita, R. B. Innis and V. W. Pike, *J. Med. Chem.*, 2008, **51**, 17–30.
8 M. R. Zhang, K. Kumata, J. Maeda, K. Yanamoto, A. Hatori, M. Okada, M. Higuchi, S. Obayashi, T. Suhara and K. Suzuki, *J. Nucl. Med.*, 2007, **48**, 1853–1861.
9 M. L. James, R. R. Fulton, J. Vercoullie, D. J. Henderson, L. Garreau, S. Chalon, F. Dollé, S. Selleri, D. Guilloteau and M. Kassiou, *J. Nucl. Med.*, 2008, **49**, 814–822.
10 N. Arlicot, J. Vercouillie, M. J. Ribeiro, C. Tauber, Y. Venel, J. L. Baulieu, S. Maia, P. Corcia, M. G. Stabin, A. Reynolds, M. Kassiou and D. Guilloteau, *Nucl. Med. Biol.*, 2012, **39**, 570–578.
11 M. Fujita, M. Imaizumi, S. S. Zoghbi, Y. Fujimura, A. G. Farris, T. Suhara, J. Hong, V. W. Pike and R. B. Innis, *Neuroimage*, 2008, **40**, 43–52.
12 F. Dollé, C. Luus, A. Reynolds and M. Kassiou, *Curr. Med. Chem.*, 2009, **16**, 2899–2923.
13 D. R. Owen, R. N. Gunn, E. A. Rabiner, I. Bennacef, M. Fujita, W. C. Kreisl, R. B. Innis, V. W. Pike, R. Reynolds, P. M. Matthews and C. A. Parker, *J. Nucl. Med.*, 2011, **52**, 24–32.
14 D. R. Owen, O. W. Howell, S. P. Tang, L. A. Wells, I. Bennacef, M. Bergstrom, R. N. Gunn, E. A. Rabiner, M. R. Wilkins, R. Reynolds, P. M. Matthews and C. A. Parker, *J. Cereb. Blood Flow Metab.*, 2010, **30**, 1608–1618.
15 A. K. Tiwari, J. Yui, M. Fujinaga, K. Kumata, Y. Shimoda, T. Yamasaki, L. Xie, A. Hatori, J. Maeda, N. Nengaki and M. R. Zhang, *J. Neurochem.*, 2014, **129**, 712–720.
16 A. Varrone, C. Steiger, M. Schou, A. Takano, S. J. Finnema, D. Guilloteau, B. Gulyás and C. Halldin, *Synapse*, 2009, **63**, 871–880.
17 M. Fujinaga, T. Yamasaki, J. Maeda, J. Yui, L. Xie, Y. Nagai, N. Nengaki, A. Hatori, K. Kumata, K. Kawamura and M. R. Zhang, *J. Med. Chem.*, 2012, **55**, 11042–11051.
18 M. Fujinaga, T. Yamasaki, J. Yui, A. Hatori, L. Xie, K. Kawamura, C. Asagawa, K. Kumata, T. Fukumura and M. R. Zhang, *J. Med. Chem.*, 2012, **55**, 2342–2352.
19 M. R. Zhang, A. Tsuchiyama, T. Haradahira, Y. Yoshida, K. Furutsuka and K. Suzuki, *Appl. Radiat. Isot.*, 2002, **57**, 335–342.
20 A. A. Wilson, J. N. Dasilva and S. S. Houle, *Appl. Radiat. Isot.*, 1995, **46**, 765–770.
21 K. Kumata, J. Yui, A. Hatori, M. Fujinaga, K. Yanamoto, T. Yamasaki, K. Kawamura, H. Wakizaka, N. Nengaki, Y. Yoshida, M. Ogawa, T. Fukumura and M. R. Zhang, *J. Med. Chem.*, 2011, **54**, 6040–6049.
22 A. Roivainen, K. Någren, J. Hirvonen, V. Oikonen, P. Virsu, T. Tolvanen and J. O. Rinne, *Eur. J. Nucl. Med. Mol. Imaging*, 2009, **36**, 671–682.
23 J. Yui, J. Maeda, K. Kumata, K. Kawamura, K. Yanamoto, A. Hatori, T. Yamasak, N. Nengaki, M. Higuchi and M. R. Zhang, *J. Nucl. Med.*, 2010, **51**, 1301–1309.
24 J. Yui, A. Hatori, K. Kawamura, K. Yanamoto, T. Yamasaki, M. Ogawa, Y. Yoshida, K. Kumata, M. Fujinaga, N. Nengaki, T. Fukumura, K. Suzuki and M. R. Zhang, *NeuroImage*, 2011, **54**, 123–130.